



# Production of sensitive gas sensors using CuO/SnO<sub>2</sub> nanoparticles

Ahmad I. Ayesh<sup>1</sup> · Aldana A. Alyafei<sup>2</sup> · Rameen S. Anjum<sup>3</sup> · Radwa M. Mohamed<sup>2</sup> · Mai B. Abuharb<sup>2</sup> · Belal Salah<sup>1</sup> · Maitha El-Muraikhi<sup>1</sup>

Received: 11 May 2019 / Accepted: 15 June 2019 / Published online: 23 July 2019  
© The Author(s) 2019

## Abstract

Metal oxide nanoparticles, such as CuO and SnO<sub>2</sub>, are outstanding systems for H<sub>2</sub>S gas sensing in air. In this work, those nanoparticles were deposited with different mixing percentages on substrates to form percolating networks of nanoparticles. Electrical electrodes were deposited on the nanoparticles' films to investigate their gas sensing response against H<sub>2</sub> and H<sub>2</sub>S, and their electrical characteristics. The sensor devices based on CuO–SnO<sub>2</sub> nanoparticles revealed enhanced sensing characteristics against H<sub>2</sub>S with a sensitivity of 10 ppm. The enhanced sensing characteristics could be attributed to the formation of PN-junctions among CuO and SnO<sub>2</sub> nanoparticles. The reasonable production cost (due to simple structure and cheap used materials), low power consumption (~ 1 μW for H<sub>2</sub>S at room temperature), high sensitivity, high response, and reasonable response time of the present sensors qualify them for practical implementation in portable gas sensing devices with enhanced characteristics.

## 1 Introduction

The recent developments in technology and industry lead to further emission of toxic gases that cause pollution to domestic environments. Some of those gases are extremely toxic and their presence, even in few tens of ppm, is a hazard to human life. Therefore, highly sensitive and selective detection of gases is required to monitor and control environment quality [1].

A conductometric gas sensor is a device that detects gaseous species in an environment by change in its electrical resistance [2, 3]. This type of sensors is attractive for utilization in portable field applications due to its many advantages that include the simple fabrication process, compact size, and direct reading [4]. The functionality of those sensors can be greatly enhanced when utilizing nanomaterials, as the sensing elements, due to their large surface to volume ratio that generates further active reaction sites [5, 6]. SnO<sub>2</sub>

nanoparticles are the main candidate used for gas sensors, however, their performance is affected by many factors, such as nanoparticle size, polycrystallinity, and operation temperature [7]. The sensing performance of those nanoparticles is vastly enhanced by the addition of another metal-oxide nanoparticle with a high affinity to the target gas.

H<sub>2</sub>S gas is a volatile gas that may be generated from different sources such as dumps, toilets, human mouth, and mainly from petroleum extraction and refining activities [8, 9]. Accurate H<sub>2</sub>S sensors are required for implementation for safety, control, and environment quality applications in the fields related to its emission. CuO modified SnO<sub>2</sub> nanoparticles is a promising system for sensitive and selective detection of H<sub>2</sub>S in the air because of the formation of PN-junctions between those semiconducting nanoparticles and the great chemical affinity of CuO nanoparticles for H<sub>2</sub>S gas [10, 11]. H<sub>2</sub>S gas is a reducing gas where its adsorption on the CuO–SnO<sub>2</sub> PN-junctions leads to the reduction of both barrier width and depletion width at the junction. Herein, the uniform desorption of CuO with SnO<sub>2</sub> nanoparticles is desirable since it allows the diffusion of H<sub>2</sub>S gas to the sensing locations on the CuO–SnO<sub>2</sub> PN-junctions.

This investigation reports on the fabrication of H<sub>2</sub>S gas sensors based on composite percolating films of CuO and SnO<sub>2</sub> nanoparticles. CuO nanoparticles are synthesized using a solvothermal method, while SnO<sub>2</sub> nanoparticles are synthesized using a sol–gel method in a microwave oven.

✉ Ahmad I. Ayesh  
ayesh@qu.edu.qa

<sup>1</sup> Department of Mathematics, Statistics and Physics, Qatar University, P. O. Box 2713, Doha, Qatar

<sup>2</sup> Chemical Engineering Department, Qatar University, Doha, Qatar

<sup>3</sup> Electrical Engineering Department, Qatar University, Doha, Qatar

The nanoparticles are dispersed in different ratios and deposited on glass slides to form percolating film of nanoparticles. A pair of parallel copper electrodes is used to investigate the electrical characteristics as well as the gas sensing properties of the produced sensors. The sensors are tested against  $H_2$  and  $H_2S$  gases where the sensitivity, response, and response time are explored. The sensors demonstrate enhanced sensing characteristics which are attributed to the formation of PN-junctions between CuO and  $SnO_2$  nanoparticles. Therefore, those sensors have the potential for implementation in practical portable gas sensing devices.

## 2 Experimental

### 2.1 Materials

$Cu(CH_3COOH)$ , NaOH, citric acid, and ethanol 99.8% were purchased from Sigma Aldrich. Acetic acid 99.5% and  $SnCl_2 \cdot 2H_2O$  were purchased from BDH.

### 2.2 Synthesis of nanoparticles

CuO nanoparticles were synthesized using a solvothermal method [12] with modification. 0.5 g of  $Cu(CH_3COOH)$  was dissolved in 0.3 ml of acetic acid by sonication, then mixed with 100 ml ethanol with a gradual increase of solution temperature to 80 °C. 10 ml of ethanol solution with 0.26 g of NaOH was added to the solution drop by drop under vigorous stirring. The color of the solution changed to black, and the solution was kept under stirring for 30 min. The nanoparticles were washed using deionized water and ethanol 5 times by a centrifuge at 6000 rpm, then dried in an oven at 60 °C overnight.

$SnO_2$  nanoparticles were synthesized using the sol-gel method inside a typical microwave oven [13]. A solution of  $SnCl_2 \cdot H_2O$  and citric acid was mixed slowly with 3:5 mol ratio without precipitate formation. The mixture was heated at 80 °C, where water started to evaporate giving a sol then gel with time. The gel was exposed to microwave radiation with a fixed power of 1.25 kW for 6 min where the gel burned. The outcome, black powder, was collected and annealed at 550 °C for 2 h with a temperature increase rate of 3 °C/min to result a white powder of  $SnO_2$  nanoparticles.

### 2.3 Sensor fabrication

Glass slides with dimensions of  $10 \times 10 \text{ mm}^2$  each were cleaned in a sonicator bath using acetone, ethanol, and deionized water. Different percentages of CuO and  $SnO_2$  nanoparticles (1:0, 0.75:0.25, 0.5:0.5, 0.25:0.75, and 0:1) were dispersed in deionized water using a sonicator bath for 10 min to obtain good mixing. A 50  $\mu\text{l}$  solution drop was

casted on a glass slide, and it was left to dry overnight in an oven at 50 °C to give a uniform layer. A holder with a pair of parallel copper electrodes with a separation of 1.5 mm was deposited on top of each film/substrate. The copper electrodes were connected to wires using silver paste to allow charge transport and sensitivity measurements. Next, the prepared device was fixed on a temperature-controlled stage inside a gas sensitivity test chamber that was made out of Teflon.

## 2.4 Characterization

An FEI scanning electron microscope (SEM) (model: Nonva NanoSEM-450) equipped with an energy dispersive X-ray spectroscopy (EDS) system was employed to identify the morphology and chemical composition of the produced nanoparticles. It should be noted here that a thin film of gold was deposited on each sample prior to SEM imaging to enhance the resolution. The composition and crystallography were further analyzed using a PANalytical X-ray diffractometer (XRD) (model: Empyrean). Herein,  $2\theta$  angle was scanned with a step size of  $0.02^\circ$  within the range  $10^\circ$ – $80^\circ$ . The measurements were conducted using the radiation peak of  $Cu-K_\alpha$  that exhibits a wavelength ( $\lambda$ ) of 1.5406 Å.

Current–voltage ( $I(V)$ ) electrical characterization technique was utilized to investigate electrical charge transport within the produced films using a source measurement unit (Keithley Instruments, SMU-236). The electrical tests were established inside the Teflon test chamber on the test stage with temperature control using a K-type thermocouple (placed on sample surface). For gas sensitivity measurements, the target gas was diluted with air using mass flow meters (Bronkhorst), then presented into the Teflon test chamber. SMU-236 was utilized to determine the electrical response of the gas by measuring the electrical current change across each sensor whereas a constant voltage was applied.

## 3 Results and discussion

The morphology and composition of the produced nanoparticles are presented in Fig. 1. The SEM images demonstrate the production of nanoparticles that form larger agglomerates. The images reveal that the sizes of CuO and  $SnO_2$  nanoparticles are  $10.0 \pm 3.3 \text{ nm}$  and  $16.2 \pm 5.4 \text{ nm}$ , respectively. The EDS composition measurements shown in Fig. 1 confirm the formation of both of CuO and  $SnO_2$  nanoparticles.

Figure 2 shows X-ray analysis of both CuO and  $SnO_2$  powder. The XRD results confirm the formation of CuO and  $SnO_2$  nanoparticles of monoclinic and tetragonal structures, respectively. The reference card used for CuO nanoparticles is ICSD-87126, and for  $SnO_2$  nanoparticles

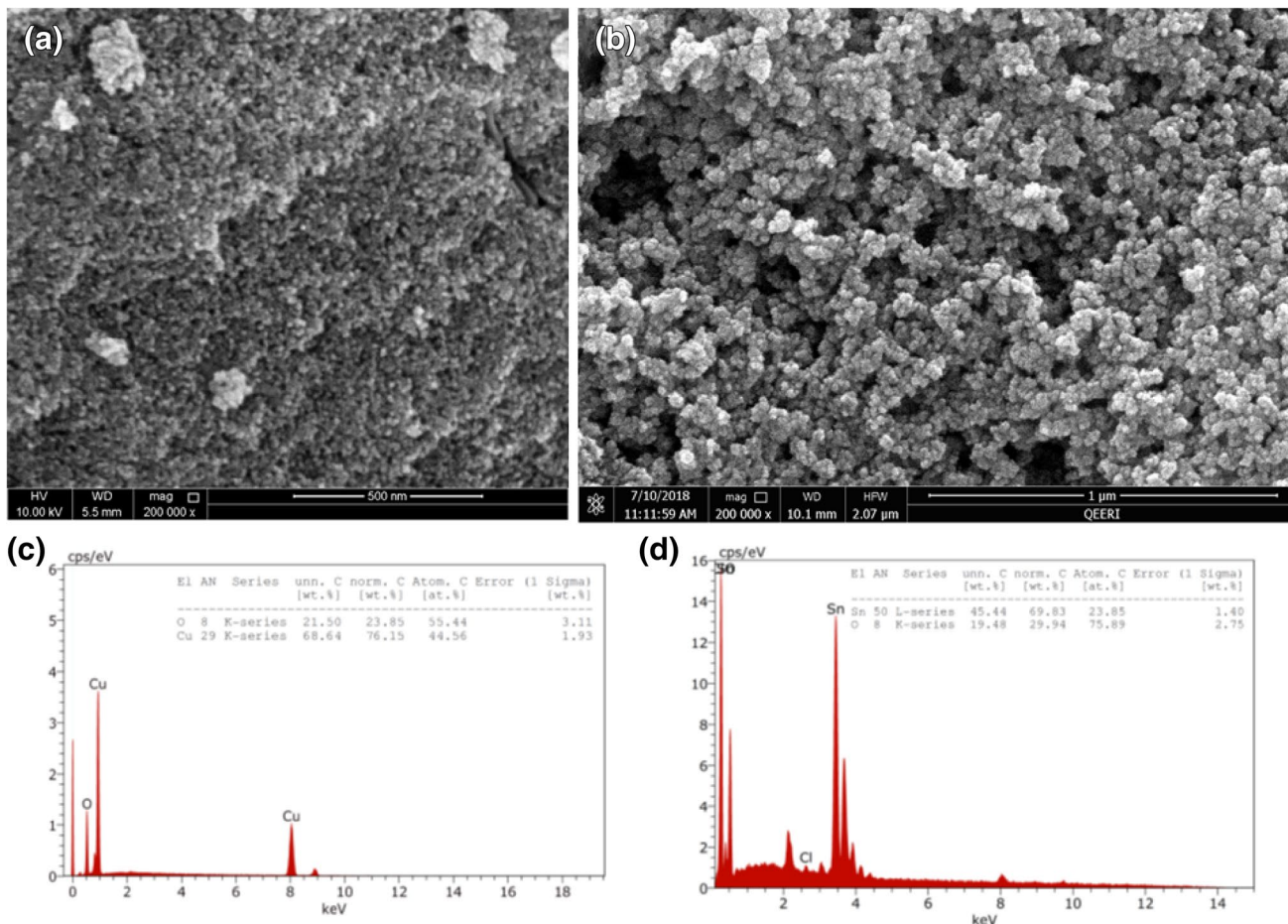


Fig. 1 SEM images of the produced CuO nanoparticles: **a** CuO and **b** SnO<sub>2</sub>. EDS measurements of the composition of nanoparticles: **c** CuO and **d** SnO<sub>2</sub>

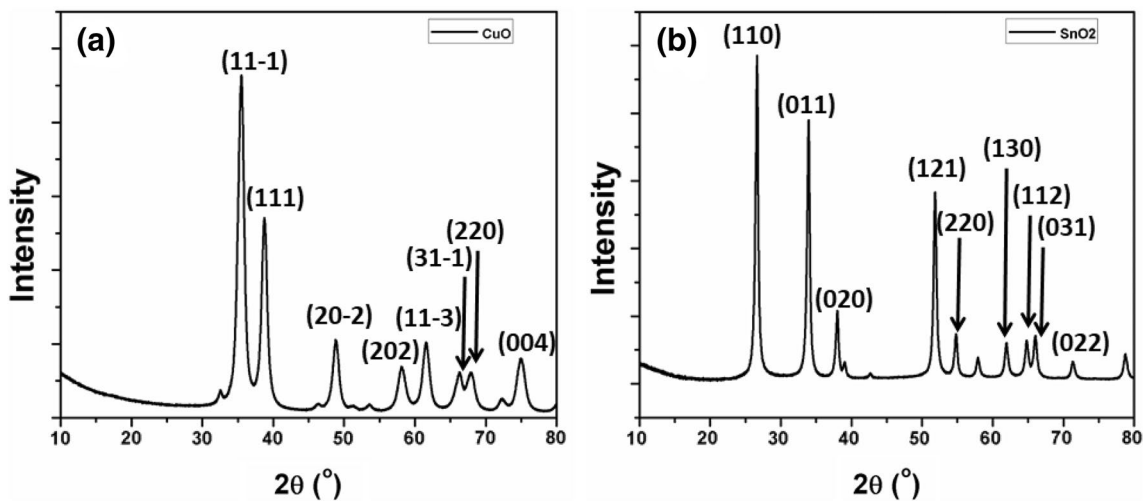


Fig. 2 XRD of the produced **a** CuO and **b** SnO<sub>2</sub> nanoparticles with Miller indices indicated on the figures

is ICSD-160667. The Miller indices are identified according to the above structures and indicated on the figures. The Sherrer’s equation can be used to estimate the nanoparticle size ( $D$ ) from XRD measurements, and presented as [14, 15]:

$$D = \frac{k\lambda}{\beta \cos \theta}$$

Here,  $k$  is set to 0.95 and it is a dimensionless constant that is assigned to nanoparticle structure,  $\lambda = 1.5406 \text{ \AA}$  and it is the wavelength of XRD radiation peak ( $\text{Cu-}K_{\alpha}$ ),  $\beta$  is defined as the full width at half maximum of an XRD peak, and  $\theta$  is the Bragg’s angle. The size calculations are established using the XRD peaks (11-1) and (110) for  $\text{CuO}$  and  $\text{SnO}_2$  nanoparticles, respectively. The  $\text{CuO}$  nanoparticle size is estimated to 7.9 nm, while the  $\text{SnO}_2$  nanoparticle size is estimated to 18.8 nm. Those values are consistent with the results obtained from the SEM images within the error bars. Furthermore, it should be noted that nanoparticles exhibit size distributions and they

form agglomerates which cause variation in the actual size estimation.

Thin films of nanoparticles are tested with the following  $\text{CuO}:\text{SnO}_2$  ratios: 1:0, 0.75:0.25, 0.5:0.5, 0.25:0.75, and 0:1. Pictures of produced films are shown in Fig. 3. Each film is tested for its electrical charge transport inside the Teflon chamber, where a holder that contains a pair of parallel copper electrodes is placed on top of the film. The test chamber and schematic diagram of the electrical measurement circuit are shown in Fig. 3.

Figure 4a shows  $I(V)$  measurements for a  $\text{CuO}$  film as a function of temperature. The figure reveals small non-linearity within the measurement voltage range and a negative temperature coefficient of the resistance. The dependence of the resistance on temperature is shown in Fig. 4b. The resistance is calculated using the linear region at low voltage (1 V). The figure confirms the negative temperature coefficient of the resistance. Furthermore, it demonstrates that the resistance is proportional directly to the percentage of  $\text{SnO}_2$  within the sample. The non-linearity could result from different reasons, for example, Schottky barriers between

**Fig. 3** Schematic diagram of the electrical measurement circuit and sample pictures of  $\text{CuO}$ ,  $\text{SnO}_2$  samples, and the Teflon test chamber

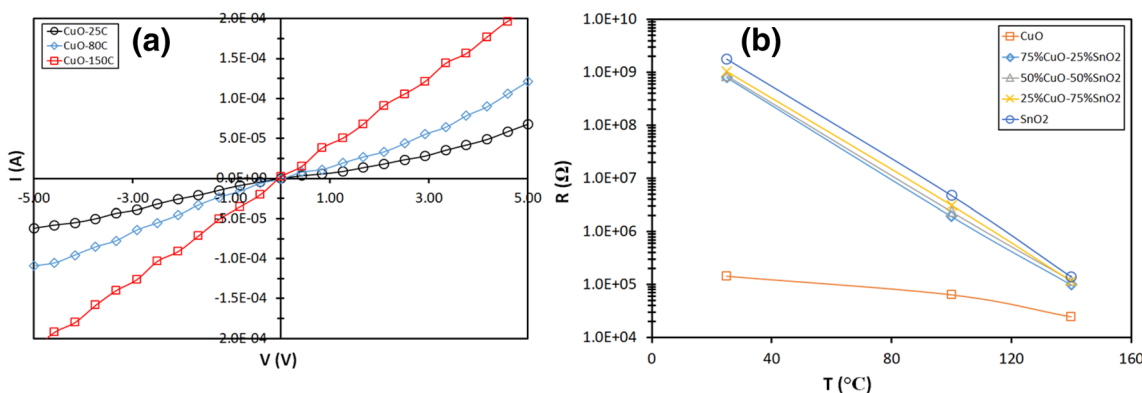
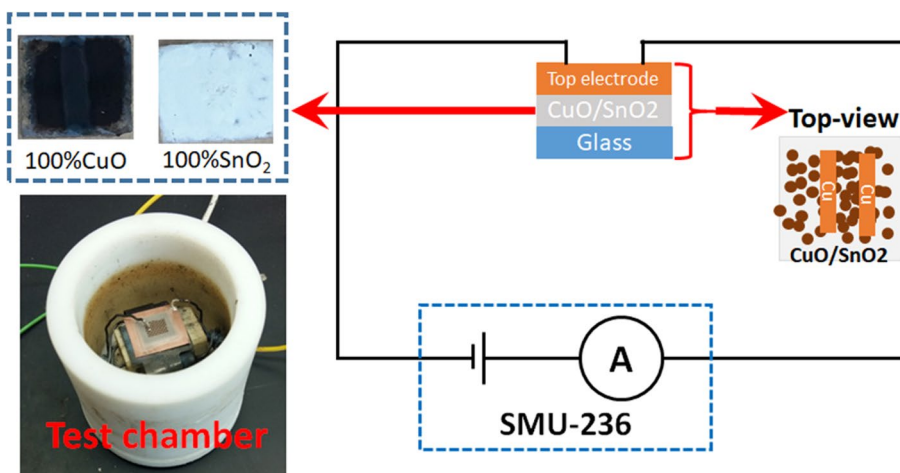


**Fig. 4** **a**  $I(V)$  as a function of temperature for the sample  $\text{CuO}:\text{SnO}_2$  ratio of 1:0. **b** The dependence of the electrical resistance on temperature for the produced sensors as a function of  $\text{CuO}:\text{SnO}_2$  ratios

metal contacts and semiconducting materials [9]. The negative temperature coefficient of the resistance was observed previously for different percolating networks of nanoparticles [8, 16, 17]. Furthermore, the results expose that sensor resistances are dominated by SnO<sub>2</sub> which is consistent with published values of resistivity:  $\rho_{\text{CuO}} = 18 \Omega \text{ m}$  [18] and  $\rho_{\text{SnO}_2} \sim 85 \Omega \text{ m}$  [19] at room temperature.

The fabricated sensors were tested for their sensitivity of H<sub>2</sub> and H<sub>2</sub>S gases. The gas response tests were established by applying a fixed bias voltage across a sensor electrodes and measuring the variation in current signal during gas exposure, see Fig. 3. A sample of the CuO sensor response results against H<sub>2</sub> gas measured at 140 °C is presented in Fig. 5a. The figure shows that when the sensor is exposed to H<sub>2</sub> gas, the electrical current increases with an amount that is proportional to H<sub>2</sub> concentration. Once H<sub>2</sub> gas is stopped and the chamber is “washed” with air, the electrical current revert back to its base value. Furthermore, the current signal tends to saturate at high H<sub>2</sub> concentrations.

The gas response of a sensor can be expressed as  $S = \left| \frac{I_{\text{gas}} - I_{\text{ref}}}{I_{\text{ref}}} \right| = \frac{|\Delta I|}{I_{\text{ref}}}$ . Here,  $I_{\text{gas}}$  is the current signal while the target gas present in the test chamber, while  $I_{\text{ref}}$  is the base current signal, i.e. with air only. Figure 5b–f present the hydrogen gas response results for the produced sensors with CuO:SnO<sub>2</sub> ratios of 1:0, 0.75:0.25, 0.5:0.5, 0.25:0.75, and 0:1. The figures reveal that the produced sensors are sensitive to a minimum H<sub>2</sub> concentration of 600 ppm. Furthermore, the response increase with H<sub>2</sub> concentration. The sensors that contain CuO nanoparticles show response at 100 °C and 140 °C, while the sensor with pure SnO<sub>2</sub> nanoparticles

function only at 140 °C. None of the sensors exhibit any response at 25 °C. This indicates the higher affinity of CuO to H<sub>2</sub> (compared with SnO<sub>2</sub>) at the lower temperatures.

Figure 6a–e show the gas response for H<sub>2</sub>S of the produced sensors with CuO:SnO<sub>2</sub> ratios of 1:0, 0.75:0.25, 0.5:0.5, 0.25:0.75, and 0:1. The figures demonstrate a minimum sensitivity of the sensors of 10 ppm and an increase in the response with H<sub>2</sub>S concentration. Therefore, those sensors are selective to H<sub>2</sub>S compared with H<sub>2</sub>. A comparison between the minimum sensitivity of previously reported sensors as well as commercial sensors is presented in Table 1. The response of the present sensors to H<sub>2</sub>S is enhanced or at least comparable with the reported values of similar system of nanoparticles [20, 21], and better in terms of their functionality at room temperature [22]. All the sensors are functional at the three measurement temperatures (except that of CuO:SnO<sub>2</sub> ratio of 0.25:0.75). At low gas concentrations, the responses of all sensors are approximately identical, while different responses are observed at high concentrations. For the sensor with CuO:SnO<sub>2</sub> ratio of 1:0, the response is almost identical regardless of the measurement temperature. For sensors with CuO:SnO<sub>2</sub> ratios of 0.75:0.25 and 0.5:0.5, the response is higher at room temperature compared to that at high temperatures. Nevertheless, for sensors with the majority of SnO<sub>2</sub> (CuO:SnO<sub>2</sub> ratios of 0.25:0.75 and 0:1), the response increase with temperature.

A sensor response time is defined as the time needed for the sensor response to cover 90% of its maximum value. The values of the response times toward both H<sub>2</sub> and H<sub>2</sub>S are shown in Table 2. Each of the presented values is the average sensor response for different gas concentrations at

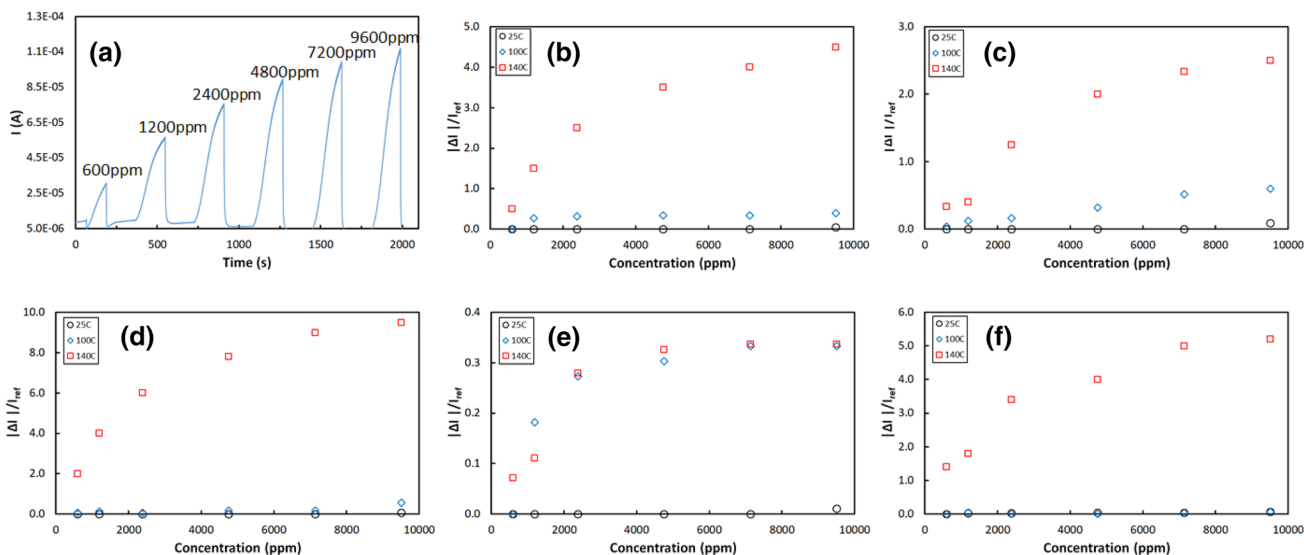


**Fig. 5** a Electrical current signal for different H<sub>2</sub> gas concentrations of CuO sensor at 140 °C measured at 1 V. Sensor response of the produced sensors against H<sub>2</sub> gas as a function of temperature and sample

composition with CuO:SnO<sub>2</sub> ratios of: **b** 1:0, **c** 0.75:0.25, **d** 0.5:0.5, **e** 0.25:0.75, and **f** 0:1

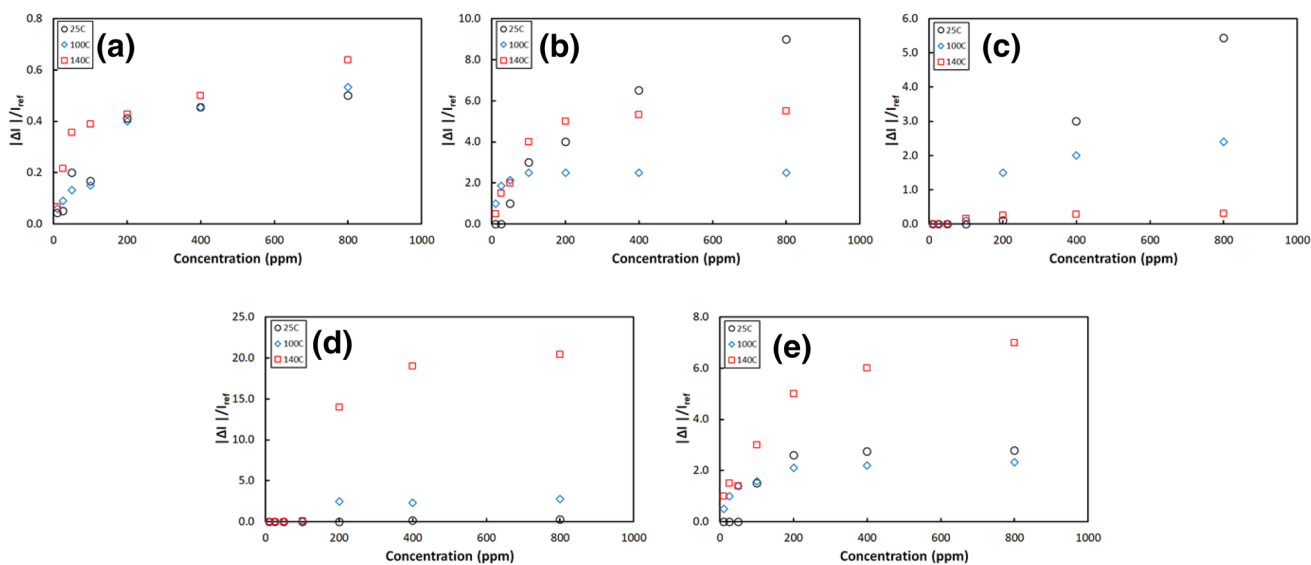


**Fig. 6** Sensor response of the produced sensors against  $\text{H}_2\text{S}$  gas as a function of temperature and sample composition with  $\text{CuO}:\text{SnO}_2$  ratios of: **a** 1:0, **b** 0.75:0.25, **c** 0.5:0.5, **d** 0.25:0.75, and **e** 0:1

**Table 1** Reported sensor response to  $\text{H}_2\text{S}$  gas

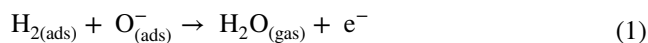
Sensor response of similar systems based on $\text{Cu}/\text{SnO}_2$	References	Sensor response of commercial sensors (ppm)	References
10 ppm @ 100 °C	[20]	25	[35]
20 ppm @ 140 °C	[21]	50	[36]
20 ppm @ 150 °C	[37]	50	[38]

**Table 2** Response times of the sensor with different compositions to  $\text{H}_2$  and  $\text{H}_2\text{S}$  gases

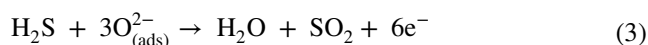
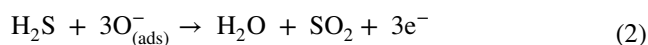
Sensor	Response time to $\text{H}_2$ gas (s)	Response time to $\text{H}_2\text{S}$ gas (s)
100% $\text{CuO}$	$41 \pm 35$	$129 \pm 58$
75% $\text{CuO}$ + 25% $\text{SnO}_2$	$44 \pm 27$	$108 \pm 48$
50% $\text{CuO}$ + 50% $\text{SnO}_2$	$19 \pm 17$	$128 \pm 58$
25% $\text{CuO}$ + 75% $\text{SnO}_2$	$94 \pm 38$	$114 \pm 31$
100% $\text{SnO}_2$	$80 \pm 38$	$132 \pm 42$

different temperatures, and the error is the standard deviation. The table shows that the sensors' response times toward  $\text{H}_2$  is lower than that toward  $\text{H}_2\text{S}$ . Furthermore, the response time toward  $\text{H}_2$  of sensors with majority  $\text{SnO}_2$  is higher than the others ( $\sim$  double), while the response time toward  $\text{H}_2\text{S}$  of all sensors is almost constant (variations are within the error). The response time values presented here are comparable with the literatures' reported values for  $\text{CuO}$  and  $\text{SnO}_2$  based sensors [9, 17, 23–25]. The lower response time towards  $\text{H}_2$  gas than  $\text{H}_2\text{S}$  can be assigned to the lower molecular weight of  $\text{H}_2$  that causes easiness of penetration and extraction.

The functionality of the sensors toward  $\text{H}_2\text{S}$  at room temperature indicates their selectivity, low power consumption ( $\sim 1 \mu\text{W}$  for  $\text{H}_2\text{S}$  at room temperature), and safe operation. The enhanced gas response of nanoparticles, in general, is typically assigned to their large surface to volume ratio. The saturation of response signal, thus, may be assigned to adsorption of the target gas on most of the reactive sites on nanoparticles' surfaces. When the surface of a metal-oxide nanoparticle is exposed to hydrogen, which is a reducing gas, its molecules react with the adsorbed oxygen species on the nanoparticle surface. Thus, electrons are re-injected to the conduction band according to the below reaction [17, 26, 27]:



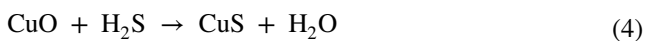
Similarly, the  $\text{H}_2\text{S}$  response of metal-oxide nanoparticles is mainly due to the high generation of charge carriers because of the adsorption of oxygen species (that include  $\text{O}^-$  and  $\text{O}^{2-}$ ) on the reactive surface sites of metal-oxide nanoparticles [28, 29]. This adsorption can be explained as [30]:



Consequently, the increase in the response of sensors when exposed to H<sub>2</sub>S gas may be allocated to the increase in free electrons according to Eqs. 2 and 3. When H<sub>2</sub>S gas is removed, no further generation of free electrons and the sensor is “washed” from H<sub>2</sub>S gas, thus, the number of free electrons as well as electrical current signal are reduced. Henceforth, the sensing process of H<sub>2</sub>S is a reversible process which permit utilizing the sensor for multiple tests. It should be noted here that the performance of those sensors is not expected to be influenced by the ambient humidity as the nanoparticles are metal oxides, and H<sub>2</sub>O is already produced upon adsorption of gas (Eqs. 1–3) without clear effect on sensor performance.

The adsorption of oxygen on pure SnO<sub>2</sub> nanoparticles release electrons and form a depletion layer near its surface. Here, electrons need further energy to be transported through the network of nanoparticles, therefore, the SnO<sub>2</sub> sensors are best functional at high temperatures.

The results in Figs. 5 and 6 reveal the improved response of the composite CuO–SnO<sub>2</sub> sensors. The major contribution to the excellent sensing characteristics here is assigned to the formation of PN-junction between CuO and SnO<sub>2</sub> that are P-type and N-type materials, respectively [10, 31]. Therefore, in Fig. 6, the composition for the optimum formation of the PN-junctions here is 0.25:0.75 for CuO:SnO<sub>2</sub>. When the nanoparticles are in the air, the PN-junctions of CuO and SnO<sub>2</sub> form barriers that reduce electron transportation through the network of nanoparticles, thus, electrical current is minimal. Once the PN-junctions are exposed to H<sub>2</sub>S, the gas reacts with CuO nanoparticles forming CuS metal [32] according [10]:



The formation of CuS metal eliminates the PN-junction. Herein, the work function of CuS is obviously less than that of SnO<sub>2</sub> [33], thus, the band bends to low energy which elements the barrier between the CuO–SnO<sub>2</sub> PN-junctions. Consequently, electrons can move freely through the junctions which increases the electrical current clearly as compared with that in the presence of air only. When the junction is exposed to air, CuS oxidizes again to CuO re-forming the CuO–SnO<sub>2</sub> junctions. Furthermore, CuS convert to Cu<sub>2</sub>S at high temperatures beyond 103 °C which exhibits a lower conductance than CuS [32]. Therefore, the CuO–SnO<sub>2</sub> junctions exhibit low sensitivity to H<sub>2</sub>S at high temperatures, as demonstrated by Fig. 6b, c. Since each sensor contains many CuO–SnO<sub>2</sub> junctions, the present sensors exhibit enhanced sensitivity as compared with their bulk equivalent.

The band structure between CuO–SnO<sub>2</sub> and electronic interface can be utilized to explain the enhanced sensing properties towards H<sub>2</sub>S gas. The band structure between CuO–SnO<sub>2</sub> is presented in Fig. 7 [34]. The SnO<sub>2</sub> bend upward at the interface due to the increase in its work

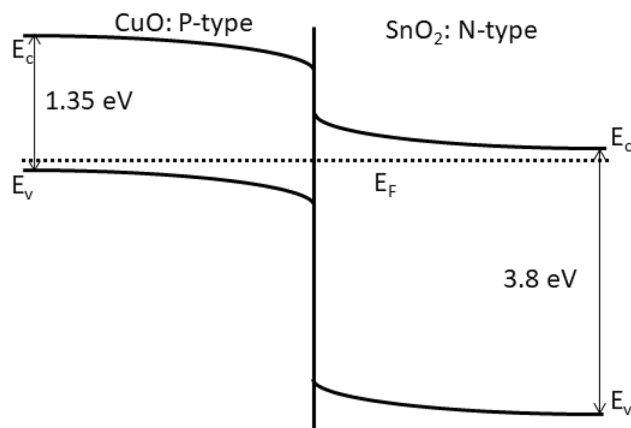


Fig. 7 Schematic diagram of the band structure for the PN junction between CuO–SnO<sub>2</sub>

function as well as the formation of layer of space charges from depleted electrons. Once the CuO–SnO<sub>2</sub> junction is exposed to H<sub>2</sub>S gas, metallic CuS is formed that leads to destroying the junction thus the band structure of SnO<sub>2</sub> returns to its pure state.

## 4 Conclusion

Hydrogen sulfide gas sensors were fabricated in this work using CuO and SnO<sub>2</sub> nanoparticles. CuO nanoparticles were produced by a solvothermal method, while SnO<sub>2</sub> nanoparticles were produced by a sol–gel method in a microwave oven. The nanoparticles were deposited with different ratios on substrates to produce percolating films of nanoparticles. The produced sensor devices based on CuO–SnO<sub>2</sub> nanoparticles were found to exhibit enhanced sensitivity and response towards H<sub>2</sub>S gas with a sensitivity of 10 ppm. The improved sensing behavior could be assigned to the production of PN-junctions between CuO and SnO<sub>2</sub> nanoparticles. The reported sensors are attractive for practical utilization in portable gas detectors due to their enhanced features that include their low production cost, functionality at room temperature, and low power consumption.

**Acknowledgements** Open Access funding provided by the Qatar National Library. This work was supported by both Qatar National Research Fund (QNRF) under a Grant Number UREP21-035-2-013, and Qatar University fund under a Grant Number QUCC-CAS-2018/2019-1. The SEM/EDS measurements were accomplished in the Central Laboratories unit at Qatar University.

**Open Access** This article is distributed under the terms of the Creative Commons Attribution 4.0 International License (<http://creativecommons.org/licenses/by/4.0/>), which permits unrestricted use, distribution, and reproduction in any medium, provided you give appropriate

credit to the original author(s) and the source, provide a link to the Creative Commons license, and indicate if changes were made.

## References

- G.A. Poda, Hydrogen sulfide can be handled safely. *Arch. Environ. Health Int. J.* **12**, 795–800 (1966)
- A.I. Ayesh, Metal/metal-oxide nanoclusters for gas sensor applications. *J. Nanomater.* **2016**, 2359019 (2016)
- A.I. Ayesh, M.A. Haija, A. Shaheen, F. Banat, Spinel ferrite nanoparticles for H<sub>2</sub>S gas sensor. *Appl. Phys. A* **123**, 682 (2017)
- M. Rosenberg, G. Kulkarni, A. Bosy, C. McCulloch, Reproducibility and sensitivity of oral malodor measurements with a portable sulphide monitor. *J. Dent. Res.* **70**, 1436–1440 (1991)
- E. Comini, G. Faglia, G. Sberveglieri, Z. Pan, Z.L. Wang, Stable and highly sensitive gas sensors based on semiconducting oxide nanobelts. *Appl. Phys. Lett.* **81**, 1869–1871 (2002)
- M. Gaidi, Nanostructured SnO<sub>2</sub> thin films: effects of porosity and catalytic metals on gas-sensing sensitivity. *Appl. Phys. A* **124**, 725 (2018)
- N. Barsan, M. Schweizer-Berberich, W. Göpel, Fundamental and practical aspects in the design of nanoscaled SnO<sub>2</sub> gas sensors: a status report. *Fresenius' J. Anal. Chem.* **365**, 287–304 (1999)
- A.F.S. Abu-Hani, F. Awwad, Y.E. Greish, A.I. Ayesh, S.T. Mahmoud, Design, fabrication, and characterization of low-power gas sensors based on organic-inorganic nano-composite. *Org. Electron.* **42**, 284–292 (2017)
- A.I. Ayesh, A.F.S. Abu-Hani, S.T. Mahmoud, Y. Haik, Selective H<sub>2</sub>S sensor based on CuO nanoparticles embedded in organic membranes. *Sens. Actuators B Chem.* **231**, 593–600 (2016)
- X. Xue, L. Xing, Y. Chen, S. Shi, Y. Wang, T. Wang, Synthesis and H<sub>2</sub>S sensing properties of CuO–SnO<sub>2</sub> core/shell pn-junction nanorods. *J. Phys. Chem. C* **112**, 12157–12160 (2008)
- M. Verma, A. Chowdhuri, K. Sreenivas, V. Gupta, Comparison of H<sub>2</sub>S sensing response of hetero-structure sensor (CuO–SnO<sub>2</sub>) prepared by RF sputtering and pulsed laser deposition. *Thin Solid Films* **518**, e181–e182 (2010)
- T. Kida, T. Oka, M. Nagano, Y. Ishiwata, X.G. Zheng, Synthesis and application of stable copper oxide nanoparticle suspensions for nanoparticulate film fabrication. *J Am Ceram Soc* **90**, 107–110 (2007)
- V. Subramanian, W.W. Burke, H. Zhu, B. Wei, Novel microwave synthesis of nanocrystalline SnO<sub>2</sub> and its electrochemical properties. *J. Phys. Chem. C* **112**, 4550–4556 (2008)
- M.A. Haija, A.I. Ayesh, S. Ahmed, M.S. Katsiotis, Selective hydrogen gas sensor using CuFe<sub>2</sub>O<sub>4</sub> nanoparticle based thin film. *Appl. Surf. Sci.* **369**, 443–447 (2016)
- A.R. Said, K. Said, F. Awwad, N.N. Qamhie, S.T. Mahmoud, M.A. Meetani, S. Tariq, A.I. Ayesh, Design, fabrication, and characterization of Hg<sup>2+</sup> sensor based on graphite oxide and metallic nanoclusters. *Sens. Actuators A Phys.* **271**, 270–277 (2018)
- A.I. Ayesh, Electronic transport in Pd nanocluster devices. *Appl. Phys. Lett.* **98**, 133108 (2011)
- A.I. Ayesh, S.T. Mahmoud, S.J. Ahmad, Y. Haik, Novel hydrogen gas sensor based on Pd and SnO<sub>2</sub> nanoclusters. *Mater Lett* **128**, 354–357 (2014)
- V. Saravanakannan, T. Radhakrishnan, Structural electrical and optical characterization of CuO thin films prepared by spray pyrolysis technique. *Int. J. ChemTech Res.* **6**, 306–310 (2014)
- R. Mariappan, V. Ponnuswamy, P. Suresh, R. Suresh, M. Raga-vendar, C. Sankar, Deposition and characterization of pure and Cd doped SnO<sub>2</sub> thin films by the nebulizer spray pyrolysis (NSP) technique. *Mater. Sci. Semicond Process.* **16**, 825–832 (2013)
- S.-W. Choi, J. Zhang, K. Akash, S.S. Kim, H<sub>2</sub>S sensing performance of electrospun CuO-loaded SnO<sub>2</sub> nanofibers. *Sens. Actuators B Chem.* **169**, 54–60 (2012)
- M.K. Verma, V. Gupta, A highly sensitive SnO<sub>2</sub>–CuO multilayered sensor structure for detection of H<sub>2</sub>S gas. *Sen. Actuators B Chem.* **166–167**, 378–385 (2012)
- Y. Zhao, X. He, J. Li, X. Gao, J. Jia, Porous CuO/SnO<sub>2</sub> composite nanofibers fabricated by electrospinning and their H<sub>2</sub>S sensing properties. *Sens. Actuators B Chem.* **165**, 82–87 (2012)
- N.S. Ramgir, C.P. Goyal, P.K. Sharma, U.K. Goutam, S. Bhattacharya, N. Datta, M. Kaur, A.K. Debnath, D.K. Aswal, S.K. Gupta, Selective H<sub>2</sub>S sensing characteristics of CuO modified WO<sub>3</sub> thin films. *Sens. Actuators B Chem.* **188**, 525–532 (2013)
- J. Liu, X. Huang, G. Ye, W. Liu, Z. Jiao, W. Chao, Z. Zhou, Z. Yu, H<sub>2</sub>S detection sensing characteristic of CuO/SnO<sub>2</sub> sensor. *Sensors* **3**, 110–118 (2003)
- Y.-J. Chen, F.-N. Meng, H.-L. Yu, C.-L. Zhu, T.-S. Wang, P. Gao, Q.-Y. Ouyang, Sonochemical synthesis and ppb H<sub>2</sub>S sensing performances of CuO nanobelts. *Sens. Actuators B Chem.* **176**, 15–21 (2013)
- B. Mondal, B. Basumatari, J. Das, C. Roychoudhury, H. Saha, N. Mukherjee, ZnO–SnO<sub>2</sub> based composite type gas sensor for selective hydrogen sensing. *Sens. Actuators B Chem.* **194**, 389–396 (2014)
- A.I. Ayesh, Linear hydrogen gas sensors based on bimetallic nanoclusters. *J. Alloy Compd.* **689**, 1–5 (2016)
- F.-N. Meng, X.-P. Di, H.-W. Dong, Y. Zhang, C.-L. Zhu, C. Li, Y.-J. Chen, Ppb H<sub>2</sub>S gas sensing characteristics of Cu<sub>2</sub>O/CuO sub-microspheres at low-temperature. *Sens. Actuators B Chem.* **182**, 197–204 (2013)
- A.H. Reshak, S. Auluck, Adsorbing H<sub>2</sub>S onto a single graphene sheet: a possible gas sensor. *J. Appl. Phys.* **116**, 103702 (2014)
- A.I. Ayesh, R.E. Ahmed, M.A. Al-Rashid, R.A. Alarrouqi, B. Saleh, T. Abdulrehman, Y. Haik, L.A. Al-Sulaiti, Selective gas sensors using graphene and CuO nanorods. *Sens. Actuators A* **283**, 107–112 (2018)
- C.S. Dandeneau, Y.-H. Jeon, C.T. Shelton, T.K. Plant, D.P. Cann, B.J. Gibbons, Thin film chemical sensors based on p-CuO/n-ZnO heterocontacts. *Thin Solid Films* **517**, 4448–4454 (2009)
- X. Kong, Y. Li, High sensitivity of CuO modified SnO<sub>2</sub> nanoribbons to H<sub>2</sub>S at room temperature. *Sens. Actuators B Chem.* **105**, 449–453 (2005)
- S. Manorama, G.S. Devi, V. Rao, Hydrogen sulfide sensor based on tin oxide deposited by spray pyrolysis and microwave plasma chemical vapor deposition. *Appl. Phys. Lett.* **64**, 3163–3165 (1994)
- J. Tamaki, T. Maekawa, N. Miura, N. Yamazoe, CuO–SnO<sub>2</sub> element for highly sensitive and selective detection of H<sub>2</sub>S. *Sens. Actuators B Chem.* **9**, 197–203 (1992)
- General moneters. <https://www.gmigasandflame.com/GM-Sensor-Response-Time.pdf>
- SPEC Sensors. <https://www.spec-sensors.com/product/h2s-sensor/>
- A. Chowdhuri, S.K. Singh, K. Sreenivas, V. Gupta, Contribution of adsorbed oxygen and interfacial space charge for enhanced response of SnO<sub>2</sub> sensors having CuO catalyst for H<sub>2</sub>S gas. *Sens. Actuators B Chem.* **145**, 155–166 (2010)
- CDS Crop. <https://www.gdscorp.com/hydrogen-sulfide>

**Publisher's Note** Springer Nature remains neutral with regard to jurisdictional claims in published maps and institutional affiliations.